Research Square

Preprints are preliminary reports that have not undergone peer review.
They should not be considered conclusive, used to inform clinical practice,
or referenced by the media as validated information.

CT Imaging Spectrum of SMARCA4-Deficient Non-Small Cell Lung Cancer: A Descriptive Case Series of 32 Patients

Xiaoyan Lei
Hainan General Hospital
Qionglian Kuang
Hainan General Hospital
Shishi Luo
Hainan General Hospital
Caiju Zhang
Hainan General Hospital
Xiaohua Zhang
Hainan General Hospital
Feng Chen
Hainan General Hospital
Kehui Liu
151098387060163.com

Haikou People's Hospital

Research Article

Keywords: SMARCA4, Non-Small Cell Lung Cancer, Thoracic Neoplasms, Tomography, X-ray Computed

Posted Date: August 10th, 2026

DOI: https://doi.org/10.21203/rs.3.rs-10464525/v1

License: This work is licensed under a Creative Commons Attribution 4.0 International License.
Read Full License

Additional Declarations: No competing interests reported.

Abstract

Background

SMARCA4-deficient non-small cell lung cancer (SMARCA4-dNSCLC) is a rare primary malignant epithelial tumour of the lungs. This study aimed to characterize the CT imaging findings and clinical features of SMARCA4-dNSCLC in a descriptive case series

Methods

The CT findings and clinical data from 32 patients with histologically confirmed SMARCA4-dNSCLC treated at Hainan General Hospital from September 2022 to August 2024 were retrospectively analysed. CT findings included location, size, density, presence of the lobulated and speculated sign, internal features, surrounding conditions, and pleural and/or pericardial effusion.

Results

Among the 32 patients, the age ranged from 33 to 84 years (median 63 years, average 63.6 ± 11 years); 28 were male (87.5%), and 4 were females (12.5%); Thirty-one patients presented with pulmonary nodules and masses (96.9%), among whom 25(78.1%) had peripherally. The tumour size ranged from 9 to 123 mm (median 34 mm, average 38.8 ± 23.4 mm). The tumour composition was solid in 28 patients (90.3%). Twenty-nine patients had the lobulated sign (93.5%), 18 had the spicule sign (58.1%), 15 had necrosis (48.4%) and 24 had the pleural contact sign (77.4%). Sixteen patients had mediastinal and hilar lymph node metastases (50%), and 21 had distant metastases (65.6%).

Conclusion

SMARCA4-dNSCLC was predominantly observed in elderly men with a heavy smoking history. On CT, the tumors commonly presented as large solid peripheral masses, usually found in the upper lobes of both lungs, with internal necrosis, lobulation, spiculation, and pleural contact. The tumours exhibit rapid growth (mean volume doubling time 55.8 days), with metastasis being common at presentation.

1. Background

The SWItch/Sucrose Non-Fermentable (SWI/SNF) complex is an evolutionarily conserved, ATP-dependent chromatin remodelling complex that coordinates transcriptional regulation, DNA repair, and cellular differentiation[1]. The SMARCA4 gene (BRG1), located on chromosome 19q13, encodes the core catalytic ATPase of this complex and functions as a potent tumour suppressor. Inactivating mutations or loss of SMARCA4 protein have been identified across a spectrum of highly aggressive malignancies[2], among which thoracic tumours constitute a distinct and clinically challenging group[3, 4].

In the thorax, SMARCA4 deficiency defines a unique subset of non-small cell lung cancer (SMARCA4-dNSCLC) that occurs predominantly in older male heavy smokers [5, 6]. At the molecular level, SMARCA4-dNSCLC is characterised by the frequent absence of canonical driver gene mutations (e.g., EGFR, ALK, ROS1, MET) and by consistently negative programmed death-ligand 1 (PD-L1) expression[5] [7] [8, 9]. Consequently, patients derive minimal benefit from targeted therapies or immunotherapy, and even conventional chemotherapy yields only marginal responses, resulting in a median overall survival of merely 4–7 months[10, 11].

Despite these advances in molecular and histopathological characterisation, the cross-sectional imaging appearance of SMARCA4-dNSCLC has received remarkably little attention. Existing radiological reports are limited to small retrospective cohorts or anecdotal case descriptions [6, 12], and a systematic CT-based characterisation is lacking. This knowledge gap is clinically consequential for two reasons. First, CT is the most widely used and accessible first-line imaging tool for lung cancer evaluation, and early recognition of a distinctive imaging pattern could prompt expedited BRG1 immunohistochemistry before molecular profiling results are available. Second, this tumour exhibits extraordinarily rapid growth and early metastatic dissemination; timely radiological suspicion may help inform clinical decision-making and potentially facilitate earlier consideration of clinical trial enrolment.

Therefore, this study aimed to (1) systematically characterise the CT findings of SMARCA4-dNSCLC in a relatively large cohort, (2) quantify tumour growth kinetics using volume doubling time, and (3) provide a reference imaging profile that may aid in raising clinical suspicion for this aggressive entity.

2. Methods

2.1 Case Data

This study was approved by the hospital Ethics Committee. Informed consent was waived due to the retrospective nature of the study. A total of 35 patients with SMARCA4-deficient NSCLC who were diagnosed via puncture biopsy, bronchial biopsy or postoperative pathological examination at Hainan General Hospital from September 2022 to August 2024 were included. The inclusion criteria were: (1) histologically confirmed NSCLC; (2) SMARCA4 (BRG1) deficiency confirmed by immunohistochemistry; (3) availability of pretreatment chest CT images in PACS. The exclusion criteria were: (1) concurrent other primary malignancies; (2) prior anticancer therapy (surgery, chemotherapy, radiotherapy, targeted therapy, or immunotherapy) before baseline CT; (3) incomplete clinical or imaging data. Of the 35 initially identified patients, three without baseline imaging data in PACS were excluded. A total of 32 patients with SMARCA4-dNSCLC were therefore included. SMARCA4 (BRG1) deficiency was confirmed by immunohistochemistry using a monoclonal antibody (clone MRQ-37), with loss of nuclear staining in > 95% of tumor cells. Detailed clinical data, including sex, age, smoking history, emphysema status, history of tuberculosis, clinical manifestations, tumour markers, clinical stages (according to the 8th edition of the AJCC staging manual), histopathological features, and imaging data, were collected. Molecular profiling for driver mutations and PD-L1 expression was performed on available tumour tissue. The

tumour was staged following confirmation of the histopathological diagnosis. Patients outcomes were obtained from the electronic medical records, PACS and telephone follow-up.

2.2 Chest CT scan protocol

Plain and enhanced chest CT scans were obtained for all 32 patients. Chest CT scans were conducted with one of the following scanners: TOSHIBA Aquilion (Toshiba, Japan), Philips icon (Philips, Netherlands), Definition Force (Siemens, German), Philips Ingenuity (Philips, Netherlands), or GE Apex (GE, America). All scans employed spiral CT volume scanning technology and were performed with the following scanning parameters: tube voltage, 120 kVp; automatic tube current technology, 40–150 mAs; pitch, 0.75-1.0; matrix, 512×512; and FOV, 200 mm×200 mm. The volume CT dose index (CTDIvol) ranged from 5 to 15 mGy. The scans were performed from the tips of the bilateral lungs to the kidneys. The patient was placed in the supine position with their hands raised, after which the scan started following deep inspiration and a breath hold. To obtain contrast-enhanced images, ioprotamine (350–370 mgI/mL) was injected intravenously with a power syringe at a rate of 2.5–3.5 mL/s. CT scans were performed 25 seconds (pulmonary arterial) and 50 seconds (delayed phase) after injection. The 1 mm thick images were transmitted to the postprocessing workstation for three-dimensional reconstruction and analysis.

2.3 CT finding evaluation

Two radiologists (with 10 years of experience in chest imaging diagnosis) independently analysed the images without knowing the results of the patient's pathological examinations. The CT image analysis include assessments of the distributions of the lesions (central, defined as localisation in the segmental or more proximal bronchi, close to the hilum; peripheral, defined as localisation in the subsegmental bronchi or beyond; and diffuse infiltration), location (left upper lobe (LUL), left lower lobe (LLL), right upper lobe (RUL), right middle lobe (RML), right lower lobe (RLL), and translobular, defined when the tumour spanned multiple lobes), size (maximum length diameter of tumour), density (pure ground glass nodule (pGGN): slightly elevation lesion density and a still-visible internal vascular shadow; mixed ground glass nodule (mGGN); both ground glass components and solid components within the tumour; solid nodule: no ground glass components and only solid soft tissue in the interior of the tumour), lobulated sign (a nodule or mass growing at different rates in all directions or blocked by surrounding structures; the contour can be a plurality of arc-shaped protrusions, and the arc-shaped interphase is a concave notch, forming a lobed shape), spicule sign (several linear shadows of varying lengths with little difference in the thickness of the far and near ends extending from the edge of a nodule or mass to the surrounding lung parenchyma, not connected to the pleura), internal characteristics of the tumour (vacuole sign: gas density shadows with a diameter of less than 5 mm in the lesion; cavity sign: gas density shadows with a diameter greater than 5 mm in the lesion; calcification: areas with a plain CT value > 70 HU; necrosis: areas with relatively low density following enhancement that do not enhance, excluding vessels and mucus, confirmed by both readers; air bronchogram sign: contrast between large air bronchi and solid lung tissue, with air bronchus branching shadows seen in areas of consolidation), peritumoral condition (obstructive pneumonia and/or atelectasis, pleural contact sign), degree of enhancement (none; mild enhancement, defined as a difference between the maximum enhancement

value of the lesion and the plain CT value below 20 HU; moderate enhancement, defined as a difference of 20 ~ 40 HU; significant enhancement, defined as a difference greater than 40 HU), pulmonary hilum and (or) mediastinal lymph node enlargement (short diameter > 10 mm), local metastasis (intrapulmonary metastasis, pleural metastasis), distant metastasis, and pleural effusion and/or pericardial effusion. For enhancement measurement, the region of interest (ROI) was placed on the most visibly enhancing solid portion of the lesion, carefully avoiding necrotic areas, vessels, and calcifications. If there was a difference in opinions between the two examiners, a third radiologist with more than 15 years of experience would analyse the CT images and provide a diagnosis.

For the six patients with serial CT scans before treatment, volume doubling time (VDT) was calculated assuming spherical geometry ($V = 4/3\pi r^3$) using the formula $VDT = t \times \log 2 / \log(Vt/V0)$, where t is the interval between scans. Given the limited number of patients with serial imaging, VDT analysis was considered exploratory.

2.4 Statistical analysis

SPSS 22.0 was used for statistical analysis. Counting data are expressed as rates and component ratios, and measurement data are expressed as the means ± standard deviations (SD) and/or median and ranges according to the distribution. Missing data were not imputed; denominators were reported for each variable accordingly.

3. Results

3.1 Clinical data

A total of 32 patients with SMARCA4-dNSCLC were included. The clinical characteristics of the patients are shown in Table 1. The ages of the 32 patients ranged from 33 to 84 years (median 63 years), with an average age of 63.6 ± 11 years; 28 patients were male (87.5%), and 4 were female (12.5%); and 22 patients (68.8%) had a history of smoking, with a duration ranging from 10 to 60 years (average 38.4 ± 13.7 years) and the number of cigarettes smoked ranging from 120 to 720 per year (average 354.5 ± 159.2 cigarettes per year). Seventeen patients (53.1%) had emphysema, and 6 patients had pulmonary tuberculosis (18.7%). Twenty-two patients (68.8%) had respiratory symptoms, including cough, sputum, shortness of breath, chest tightness, haemoptysis and dyspnoea; 5 patients (15.6%) had nonspecific symptoms, including dizziness, vomiting, abdominal pain, and limb and joint pain; and 5 patients (15.6%) had no symptoms. Among the 32 patients with SMARCA4-dNSCLC, 27 underwent tumour marker assessment; 5 patients (18.5%) had elevated CYFRA21-1 levels (13.02–63.06 ng/ml; reference value: 0 ~ 3.3 ng/ml), 12 patients (44.4%) had elevated CEA levels (5.05–200.12 ng/ml; reference value: 0 ~ 5 ng/ml), 4 patients (14.8%) had elevated CA19-9 levels (47.74–360.22 U/ml; reference value: 0.1–35 U/ml), and 1 patient (3.7%) had elevated neuron-specific enolase (NSE) levels (20.67 ng/ml; reference value: 0 ~ 16.3 ng/ml). Eight patients (25%) had clinical stage I disease, 2 patients (6.2%) had stage II disease, 7 (21.9%) had stage III disease, and 15 (46.9%) had stage IV disease.

Table 1
Clinical characteristics of patients with SMARCA4-dNSCLC

Characteristics	N (%)/mean ± SD
Age (years), mean ± SD	63.6 ± 11
Sex, n (%)	
Male	28 (87.5%)
Female	4 (12.5%)
Smoking history, n (%)	22 (68.8%)
Smoking duration (years), mean ± SD	38.4 ± 13.7
Smoking quantity (cigarette/year), mean ± SD	354.5 ± 159.2
Emphysema, n (%)	17 (53.1%)
Pulmonary tuberculosis, n (%)	6 (18.7%)
Symptom, n (%)	
Respiratory symptoms	22 (68.8%)
Nonspecific symptoms	5 (15.6%)
No symptoms	5 (15.6%)
Tumour markers[a], n (%)	
CYFRA21-1	5 (18.5%)
CEA	12 (44.4%)
CA199	4 (14.8%)
NSE	1 (3.7%)
Clinical stage, n (%)	
Stage I	8 (25%)
Stage II	2 (6.3%)
Stage III	7 (21.9%)
Stage IV	15 (46.8%)

Note: SD, standard deviation; CYFRA21 1, cytokeratin 19 fragment; CEA, carcinoma embryonic antigen; CA199, carbohydrate antigen 19 – 9; NSE, neuron specific enolase; a indicated some patients were missing these data.

3.2 CT findings

The pretreatment CT findings are shown in Table 2. Among the 32 patients, 31 presented with pulmonary nodules and masses (96.9%), among whom 25 (78.1%) had peripheral, 6 (18.8%) had central, and 1 presented with diffuse infiltration lesions (3.1%). Among these 31 patients with nodules and masses, 12 (38.7%) had lesions in the LUL, 4 (12.9%) had lesions in the LLL, 7 (22.6%) had lesions in the RUL, 0 (0%) had lesions in the RML, 5 (16.1%) had lesions in the RLL, and 4 patients had translobular lesions (3 (9.7%) with lesions across the RLL and RUL, and 1 (3.2%) with a lesion across the LUL and LLL). The tumour size ranged from 9 to 123 mm (median 34 mm), with an average of 38.8 ± 23.4 mm. In 6 patients with no follow-up treatment and with serial imaging, the tumours showed rapid short-term growth, with a volume doubling time (VDT) ranging from 22–121 days (mean 55.8 ± 37.5 days). The 6 patients with VDT analysis did not differ significantly from the overall cohort in age, sex, or stage. The tumour density was characterized as solid in 28 patients (90.3%) and partially solid in 3 patients (9.7%). Twenty-nine patients had the lobulated sign (93.5%), 18 had the spicule sign (58.1%), 1 had the air bronchogram sign (3.2%), 15 had necrosis (48.4%), 1 had cavitation (3.2%), 3 had calcification (9.7%), 24 had the pleural contact sign (77.4%), 8 had obstructive pneumonia (25.8%) and 4 had obstructive atelectasis (12.9%). Seventeen patients exhibited mild enhancement (54.8%), whereas 14 patients exhibited moderate enhancement (45.2%). Among the 32 patients, 16 had mediastinal and hilar lymph node metastases (50%), 2 had intrapulmonary metastases, 3 had pleural metastases, 21 had distant metastases (65.6%), including in the bone in 8 patients (25%), the adrenal glands in 5 patients (20%), the distant lymph nodes in 4 patients (12.5%), the brain in 3 patients (9.4%), and the liver in 1 patient (3.1%). Moreover, pleural effusion was observed in 8 patients (25%), and pericardial effusion was observed in 8 patients (25%).

Table 2
CT findings of SMARCA4-dNSCLC patients

CT findings	N (%)/mean ± SD
Distribution, n (%)	25 (78.1%)
Peripheral	5 (18.8%)
Central	1 (3.1%)
Diffuse infiltration	
Location, n (%)	12 (38.7%)
LUL	4 (12.9%)
LLL	7 (22.6%)
RUL	0 (0.0%)
RML	5 (16.1%)
RLL	3 (9.7%)
Translobular; across the RLL and RUL	1 (3.2%)
Translobular; across the LLL and LUL	38.8 ± 23.4
Tumour size (mm), mean ± SD	55.8 ± 37.5
Doubling time (days), mean ± SD	
Density, n (%)	28 (90.3%)
Solid	3 (9.7%)
Partially solid	29 (93.5%)
Lobulated sign, n (%)	18 (58.1%)
Spicule sign, n (%)	
Internal characteristics, n (%)	0 (0.0%)
Vacuole sign	1 (3.2%)
Cavity sign	3 (9.7%)
Calcification	15 (48.4%)
Necrosis	1 (3.2%)
Air bronchogram sign	
Peritumoral condition, n (%)	24 (77.4%)

Note: SD, standard deviations;LUL, left upper lobe; LLL, left lower lobe; RUL, right upper lobe; RML, right middle lobe; RLL, right lower lobe.

CT findings	N (%)/mean ± SD
Pleural contact sign	4 (12.9%)
Obstructive atelectasis	8 (25.8%)
Obstructive pneumonia	
Degree of enhancement, n (%)	17 (54.8%)
Mild	14 (45.2%)
Moderate	16 (50%)
Mediastinal and hilar lymph node metastases, n (%)	2 (6.3%)
Local metastases, n (%)	3 (9.4%)
Intrapulmonary metastases	8 (25%)
Pleural metastases	8 (25%)
Pleural effusion, n (%)	
Pericardial effusion n (%)	8 (25%)
Distant metastases, n (%)	5 (20%)
Bone	4 (12.5%)
Adrenal glands	3 (9.4%)
Lymph node	1 (3.1%)
Brain	
Liver	
CT findings	N (%)/mean ± SD
Distribution, n (%)	25 (78.1%)
Peripheral	5 (18.8%)
Central	1 (3.1%)
Diffuse infiltration	12 (38.7%)
Location, n (%)	4 (12.9%)
LUL	7 (22.6%)
LLL	0 (0.0%)
RUL	5 (16.1%)
RML	3 (9.7%)

Note: SD, standard deviations;LUL, left upper lobe; LLL, left lower lobe; RUL, right upper lobe; RML, right middle lobe; RLL, right lower lobe.

CT findings	N (%)/mean ± SD
RLL	1 (3.2%)
Translobular; across the RLL and RUL	38.8 ± 23.4
Translobular; across the LLL and LUL	55.8 ± 37.5
Tumour size (mm), mean ± SD	28 (90.3%)
Doubling time (days), mean ± SD	3 (9.7%)
Density, n (%)	29 (93.5%)
Solid	18 (58.1%)
Partially solid	0 (0.0%)
Lobulated sign, n (%)	1 (3.2%)
Spicule sign, n (%)	3 (9.7%)
Internal characteristics, n (%)	15 (48.4%)
Vacuole sign	1 (3.2%)
Cavity sign	24 (77.4%)
Calcification	4 (12.9%)
Necrosis	8 (25.8%)
Air bronchogram sign	17 (54.8%)
Peritumoral condition, n (%)	14 (45.2%)
Pleural contact sign	16 (50%)
Obstructive atelectasis	2 (6.3%)
Obstructive pneumonia	3 (9.4%)
Degree of enhancement, n (%)	8 (25%)
Mild	8 (25%)
Moderate	8 (25%)
Mediastinal and hilar lymph node metastases, n (%)	5 (20%)
Local metastases, n (%)	4 (12.5%)
Intrapulmonary metastases	3 (9.4%)
Pleural metastases	1 (3.1%)
Pleural effusion, n (%)	

Note: SD, standard deviations;LUL, left upper lobe; LLL, left lower lobe; RUL, right upper lobe; RML, right middle lobe; RLL, right lower lobe.

CT findings	N (%)/mean ± SD
Pericardial effusion n (%)	
Distant metastases, n (%)	
Bone	
Adrenal glands	
Lymph node	
Brain	
Liver	

Note: SD, standard deviations;LUL, left upper lobe; LLL, left lower lobe; RUL, right upper lobe; RML, right middle lobe; RLL, right lower lobe.

3.3 Pathological features

Among the 32 patients with SMARCA4-dNSCLC, adenocarcinoma (21 patients, 65.6%) was the most common pathological type, followed by sarcomatoid carcinoma (2 patients, 6.3%), large cell carcinoma (1 patient, 3.1%), squamous cell carcinoma (1 patient, 3.1%) and large cell neuroendocrine carcinoma (1 patient, 3.1%). Another 6 patients (18.6%) were diagnosed with nonspecific NSCLC. Of note, all SMARCA4-deficient adenocarcinomas were solid-predominant, poorly differentiated tumours, and the diagnosis was confirmed by the absence of TTF-1 and Napsin A expression to exclude conventional lung adenocarcinoma. Targeted driver gene detection was performed for 12 patients: 3 patients (25%) presented with mutations, including an EGFR gene mutation in 2 patients and a KRAS gene mutation in 1 patient. These 3 patients all presented with adenocarcinomas; none of the remaining patients demonstrated any gene mutations. The expression of PD-L1 was negative in the entire cohort (assessed using the 22C3 assay, with TPS < 1% defined as negative).

3.4 Treatment and outcomes

Among the 32 patients with SMARCA4-dNSCLC, 21 received clinical treatment, including 1 who received surgically assisted chemotherapy (stage III), 11 who underwent surgery only (7 patients with stage I, 1 patient with stage II, and 3 patients with stage III disease), 7 who received chemotherapy, 3 who received targeted therapy, 5 who received immunotherapy, and 11 who received no treatment (Fig. 1). As of November 2024, 24 patients had complete follow-up data (range 2–24 months, average 9 months). Among the 24 patients, 5 died, all of whom were in advanced stages (1 patient with stage III and 4 with stage IV disease; Fig. 2), 9 demonstrated disease progression (Fig. 3 **and** Fig. 4), and 10 were still alive and showed no disease progression.

4. Discussion

The present study systematically described the CT imaging features and clinical characteristics of 32 patients with histologically confirmed SMARCA4-deficient non-small cell lung cancer (SMARCA4-dNSCLC). To our knowledge, this is the largest imaging series to date that provides the first direct quantification of volume doubling time (mean 55.8 days) and highlights the exceptionally high prevalence of necrosis (48.4%) and pleural contact (77.4%) in this entity. The profile that emerges—a peripheral, solid, lobulated mass with internal necrosis and pleural contact, coupled with a median VDT of under two months—offers a distinct radiologic signature that, when combined with a history of heavy smoking, should raise strong suspicion for SMARCA4 deficiency.

The clinical profile of our cohort was remarkably consistent with previous reports[5, 10, 11]. The median age was 63 years, and 87.5% of patients were male, with 68.8% having a heavy smoking history (mean 38.4 pack-years). These demographic features closely mirror the clinicopathologic series by Chen et al. [5], which also identified striking male predominance and heavy tobacco exposure as hallmarks of SMARCA4/BRG1-deficient NSCLC. Concurrent emphysema was present in 53.1% of cases in our cohort, reinforcing the strong association between SMARCA4 deficiency and smoking-related lung damage, a finding consistent with a 2026 mini-review which noted that SMARCA4-deficient thoracic tumors predominantly occur in older male smokers and frequently arise on a background of smoking-related lung injury[4]. Although these demographic features are not entirely specific, they provide an important clinical context: when a heavy-smoking elderly male presents with a rapidly enlarging lung mass displaying aggressive CT features, SMARCA4-dNSCLC should be included in the differential diagnosis.

On CT, nearly all lesions (96.9%) were peripheral (78.1%), solid (90.3%) masses (mean 38.8 mm) with frequent lobulation (93.5%), spiculation (58.1%), pleural contact (77.4%), and internal necrosis (48.4%). These imaging hallmarks reflect underlying biology: peripheral location suggests derivation from small airways or alveolar epithelium and facilitates early pleural invasion; lobulation and spiculation indicate uneven growth and desmoplastic stromal reaction; pleural contact correlates with high local aggressiveness, consistent with the frequent chest wall invasion noted in prior CT series [6, 12]. Notably, the mild-to-moderate contrast enhancement and the high necrosis rate likely reflect a hypovascular, hypoxic tumour microenvironment, necrosis reflecting SWI/SNF complex dysfunction-driven genomic instability and rapid proliferation outstripping blood supply[13], contrast enhancement was only mild or moderate (54.8% and 45.2%, respectively), with no avid enhancement, suggesting a relatively hypovascular phenotype. This phenomenon is increasingly linked to the immunologically “cold” phenotype of SMARCA4-deficient tumours, as SMARCA4 loss impairs chromatin accessibility at innate immune genes (e.g., STING, IL1β), reducing dendritic cell and T-cell infiltration [14]. The limited enhancement therefore provides a radiological correlate to the immune-cold state and the poor response to immunotherapy observed clinically[15].

In six untreated patients with serial CT scans, tumour volume doubling times ranged from 22 to 121 days (mean 55.8 days). To our knowledge, this is the first direct quantification of growth kinetics in SMARCA4-dNSCLC, confirming its extreme aggressiveness and explaining the high rates of early metastasis (65.6% distant, 50% nodal) and stage IV disease (46.9%) at diagnosis. Such rapid growth

aligns with the reported median overall survival of 4–7 months[5, 11] [16, 17]. Of note, our cohort included four female and five asymptomatic patients, indicating a broader clinical spectrum than previously appreciated; thus, the absence of typical risk factors (male, heavy smoker, symptoms) should not preclude consideration of SMARCA4-dNSCLC when CT shows aggressive features. Systematic CT characterization of this entity remains limited; our study provides a comprehensive radiological profile with novel quantitative growth data and highlights necrosis and pleural contact as particularly prominent—and perhaps prognostically informative—features.

One of the most alarming findings was the high prevalence of metastatic disease at the time of diagnosis. Mediastinal or hilar lymph node metastases were present in 50% of patients, and distant metastases were detected in 65.6%, most frequently involving the bones (25%), adrenal glands (20%), distant lymph nodes (12.5%), brain (9.4%), and liver (3.1%). Nearly half of the patients (46.9%) were classified as stage IV at initial presentation. SMARCA4 loss promotes lineage dedifferentiation and increases metastatic incidence by impairing SWI/SNF chromatin remodeling function, which reduces accessibility to lung-lineage transcriptional programs and accelerates tumor progression toward a highly metastatic state[18]. This pattern indicates exceptionally aggressive biological behavior, far exceeding that of most common NSCLC subtypes. The presence of early and widespread metastases on baseline CT underscores the need for meticulous scrutiny of subtle deposits, particularly in the bones and adrenal glands, as their presence dramatically alters staging and management.

Histopathologically, adenocarcinoma was the dominant subtype (65.6%), followed by rare sarcomatoid, large cell, and other carcinomas. It is essential to clarify that all of these adenocarcinomas were solid-predominant, poorly differentiated tumours, and the diagnosis of SMARCA4-deficient adenocarcinoma was strictly established by the loss of BRG1 expression in the absence of TTF-1 and Napsin A, thereby distinguishing them from conventional well-differentiated adenocarcinomas. This explains the seemingly paradoxical co-occurrence of an adenocarcinoma histology with an undifferentiated, aggressive phenotype. Driver gene mutations were infrequent—among 12 tested patients, only 3 harbored mutations (two EGFR, one KRAS)—and PD-L1 expression was uniformly negative. These findings are consistent with recent large-cohort studies [19, 20]. The uniformly negative PD-L1 expression in our cohort aligns with the emerging understanding that SMARCA4 loss disrupts chromatin remodeling and impairs antigen presentation, fostering a poorly immunogenic tumor phenotype [9]. Mechanistically, SMARCA4 deficiency causes cancer cell-intrinsic reprogramming of the enhancer landscape with marked loss of chromatin accessibility at innate immune genes (e.g., STING, IL1β), leading to reduced infiltration of dendritic cells and CD4 + T cells into the tumor microenvironment—a basis for the immunologically “cold” phenotype and poor response to immunotherapy [14]. The paucity of actionable targets and immune-cold TME likely contribute to the limited efficacy of conventional therapies. Although some early-stage patients underwent surgical resection, outcomes remained poor: all five deaths occurred in advanced-stage patients, and nine additional patients progressed. These findings reinforce SMARCA4 deficiency as a strong adverse prognostic factor. From a radiological perspective, the constellation of a large, necrotic, peripheral solid mass with early widespread metastases in a heavy smoker should

prompt pathologists to evaluate SMARCA4/BRG1 status by immunohistochemistry, even without classic undifferentiated morphology [20].

The differential diagnosis of SMARCA4-dNSCLC on CT primarily includes conventional lung adenocarcinoma, SMARCA4-deficient undifferentiated tumor (SMARCA4-UT), squamous cell carcinoma, large cell neuroendocrine carcinoma, and sarcomatoid carcinoma. Conventional lung adenocarcinoma shares peripheral location, lobulation, and spiculation, but typically contains ground-glass components, shows less extensive necrosis, and enhances more avidly—features that help distinguish it from the solid, heavily necrotic, hypovascular SMARCA4-dNSCLC. SMARCA4-UT is the most challenging mimicker: both entities share loss of BRG1 expression and aggressive behavior [12], and on CT, SMARCA4-UT typically appears as a large invasive mass with marked heterogeneity, necrosis or cavitation, multi-structure invasion, and conglomerated lymphadenopathy [21]—features that substantially overlap with SMARCA4-dNSCLC and cannot be reliably differentiated by imaging alone. However, in our series, mediastinal lymphadenopathy from SMARCA4-dNSCLC manifested as discrete enlarged nodes rather than the confluent, “armor-like” masses described in some SMARCA4-UT cases, which may represent a subtle distinguishing clue, although this requires prospective validation. Squamous cell carcinoma, though common in smokers, is usually centrally located and frequently cavitates, in contrast to the predominantly peripheral non-cavitated SMARCA4-dNSCLC. Large cell neuroendocrine carcinoma and sarcomatoid carcinoma may exhibit bulky size and necrosis, but their imaging features are largely nonspecific and overlap with SMARCA4-dNSCLC. Thus, while certain CT features—peripheral location, solid consistency, extensive necrosis, and rapid growth—strongly suggest SMARCA4 deficiency, definitive distinction from several of these entities requires immunohistochemical confirmation. Radiologists should raise suspicion when a peripheral solid necrotic mass with aggressive features occurs in a heavy smoker, prompting targeted pathological workup including BRG1 staining.

Several limitations of this study should be acknowledged. First, the sample size of 32 patients, although relatively large for this rare disease, remains limited and may restrict the generalizability of our findings. Second, the retrospective, single-center design introduces inevitable selection bias, and treatment regimens were heterogeneous, which precludes meaningful survival analysis. Third, a control group of SMARCA4-proficient NSCLC was not included, so the specificity of the described CT features cannot be formally assessed. Fourth, the follow-up duration was relatively short (median 9 months), and some patients were lost to follow-up, limiting the evaluation of long-term outcomes. Fifth, CT acquisition parameters and contrast injection protocols varied slightly across different scanners, which could have influenced the assessment of enhancement degree and necrosis. Future prospective, multicenter studies with larger cohorts and a control group are warranted to validate these findings. Incorporating radiomics or deep learning approaches may further help build non-invasive predictive models for SMARCA4 deficiency, aiding in early risk stratification and treatment planning. highlighting a promising direction for future imaging research.

5. Conclusion

SMARCA4-dNSCLC is a highly aggressive subtype of non-small cell lung cancer predominantly affecting elderly male heavy smokers. On CT, it typically presents as a large, solid, peripherally located mass with lobulated and spiculated margins, internal necrosis, pleural contact, and mild to moderate contrast enhancement. A notable feature is its extremely rapid growth, with a mean volume doubling time of less than two months. Early lymph node and distant metastases are remarkably common. When these imaging features are encountered in a heavy-smoking patient with negative driver gene mutations and negative PD-L1 expression, the possibility of SMARCA4-dNSCLC should be strongly considered, and timely pathological confirmation with appropriate immunohistochemistry is recommended. Multicenter prospective studies are needed to further validate these findings and explore the potential of imaging biomarkers in the management of this rare entity.

Abbreviations

CA19-9
Carbohydrate antigen 19 – 9
CEA
Carcinoembryonic antigen
CT
Computed tomography
CYFRA21-1
Cytokeratin 19 fragment
LLL
Left lower lobe
LUL
Left upper lobe
mGGN
Mixed ground glass nodule
NSCLC
Non-small cell lung cancer
NSE
Neuron-specific enolase
PACS
Picture Archiving and Communication System
PD-L1
Programmed death-ligand 1
pGGN
Pure ground glass nodule
RLL
Right lower lobe
RML

Right middle lobe
RUL
Right upper lobe
SD
Standard deviation
SMARCA4-dNSCLC
SMARCA4-deficient non-small cell lung cancer
SWI/SNF
SWItch/Sucrose Non-Fermentable complex
VDT
Volume doubling time.

Declarations

Ethics approval and consent to participate

The studies involving humans were approved by the Ethics Committee of Hainan Provincial People's Hospital (No. [2025]187). The studies were conducted in accordance with the local legislation and institutional requirements. Written informed consent for participation was not required from the participants or the participants' legal guardians/next of kin because the Ethics Committee waived the requirement due to the retrospective, anonymized nature of the study.

Consent for publication

Not applicable.

Competing interests

The authors declare that the research was conducted in the absence of any commercial or financial relationships that could be construed as a potential conflict of interest.

Funding

This work was supported by Joint Program on Health Science & Technology Innovation of Hainan Province (No. WSJK2024QN078, No. WSJK2026QN176).

Author Contribution

XL and QK contributed equally to this work as co-first authors. XL, FC, and KH conceived and designed the study. XL, QK, SL, XZ, and CZ acquired the clinical and imaging data. XL, QK, and FC analyzed and

interpreted the CT imaging data. QK, SL, and XZ performed the statistical analysis and volume doubling time calculations. XL and QK drafted the initial manuscript. XZ, CZ, FC, and KH critically revised the manuscript for important intellectual content. FC and KH supervised the study and provided administrative support. All authors read and approved the final manuscript.

Acknowledgments

None

Data Availability

The datasets generated and analyzed during the current study are not publicly available due to patient confidentiality and privacy regulations, but are available from the corresponding author (Kehui Liu) on reasonable request.

References

1. Mittal P, Roberts C. The SWI/SNF complex in cancer - biology, biomarkers and therapy. NAT REV CLIN ONCOL. 2020;17(7):435–48.
2. Mardinian K, Adashek JJ, Botta GP, Kato S, Kurzrock R. SMARCA4: Implications of an Altered Chromatin-Remodeling Gene for Cancer Development and Therapy. MOL CANCER THER. 2021;20(12):2341–51.
3. Das S, Mishra P, Ahlawat S. Clinicopathological and molecular perspectives on thoracic SMARCA4-deficient undifferentiated tumors and SMARCA4-deficient non-small cell lung carcinomas. PATHOLOGICA. 2025;117(5):455–67.
4. Lin X, Ji Y, Lin B, Yang Z, Xie R. SMARCA4-deficient non-small cell lung cancer and immunotherapy resistance: mechanisms and novel strategies-a mini-review. Discover Oncol. 2026;17(1):544.
5. Chen D, Zhang H, Wang D, Ye W, Zhao H, Zhang C, Wu S, Shi Q. Clinicopathological and Genomic Analysis of SMARCA4-Deficient Non-Small Cell Lung Cancer: A Retrospective Cohort Study. CANCER MANAG RES. 2026;18:565394.
6. Wumener X, Ye X, Zhang Y, E T, Zhao J, Liang Y, Zhao J. SMARCA4/BRG1-deficient non-small cell lung cancer: clinical, imaging, pathological features, and follow-up results of 23 patients. TRANSL LUNG CANCER R. 2025;14(1):107–23.
7. Han L, Chen L, Wang L. Clinicopathological features of SMARCA4-deficient non-small cell lung cancer. Pathol Res Pract. 2025;275:156241.
8. Liu Y, Li H, Li X, Cui H, Li R, Zhu J, Cui H, Liu Y, Cheng Y. Clinicopathological characteristics and therapeutic outcomes in patients with non-small cell lung cancer harboring SMARCA4 mutations. ANN MED. 2026;58(1):2620201.

9. Paredes R, Borea R, Drago F, Russo A, Nigita G, Rolfo C. Genetic drivers of tumor microenvironment and immunotherapy resistance in non-small cell lung cancer: the role of KEAP1, SMARCA4, and PTEN mutations. J IMMUNOTHER CANCER. 2025;13(8):e12288.
10. Li SL, Wu CY, Zhang LP, Huang Y, Wu W, Zhang W, Hou LK. Clinicopathological features and prognosis of SMARCA4-deficient non-small cell lung carcinoma: an analysis of 127 cases. Zhonghua bing li xue za zhi = Chin J Pathol. 2023;52(7):665–70.
11. Zhang B, Yang X, Jia J. Clinical and pathological characteristics and prognostic factors of SMARCA4-deficient non-small cell lung cancer. ANN DIAGN PATHOL. 2025;78:152499.
12. Kim JH, Woo JH, Lim CY, An T, Han J, Chung MJ, Cha YK. SMARCA4-deficient non-small cell lung carcinoma: clinicodemographic, computed tomography, and positron emission tomography-computed tomography features. J THORAC DIS. 2024;16(3):1753–64.
13. Zhou P, Fu Y, Tang Y, Jiang L, Wang W. Thoracic SMARCA4-deficient tumors: a clinicopathological analysis of 52 cases with SMARCA4-deficient non-small cell lung cancer and 20 cases with thoracic SMARCA4-deficient undifferentiated tumor. PEERJ. 2024;12:e16923.
14. Wang Y, Meraz IM, Qudratullah M, Kotagiri S, Han Y, Xi Y, Wang J, Akdemir KC, Roth JA, Lissanu Y. Mutation of SMARCA4 Induces Cancer Cell-Intrinsic Defects in the Enhancer Landscape and Resistance to Immunotherapy. CANCER RES. 2025;85(11):1997–2013.
15. Zhang P, Kuang Y, Jia B, Tian Z, Deng M, Nie J, Dai L, Dong B, Yang X, Long M, et al. SMARCA4-deficient thoracic tumors exhibit an immunosuppressive microenvironment and respond to combined antiangiogenic and immune checkpoint inhibitor therapy. Lung cancer (Amsterdam Netherlands). 2026;217:109417.
16. Zhang M, Dong Y, Meng R, Zhang D. SMARCA4 Deficiency in Lung Cancer: From Signaling Pathway to Potential Therapeutic Targets. Genes Chromosomes Cancer. 2025;64(1):e70022.
17. Chen L, Su C, Yao J, Li X, Lin X. Retrospective Insights into the Clinicopathological Features and Treatment Outcomes of Thoracic SMARCA4-Deficient Tumors. TECHNOL CANCER RES T. 2025;24:2050880031.
18. Concepcion CP, Ma S, LaFave LM, Bhutkar A, Liu M, DeAngelo LP, Kim JY, Del PI, Schoenfeld AJ, Miller M, et al. Smarca4 Inactivation Promotes Lineage-Specific Transformation and Early Metastatic Features in the Lung. CANCER DISCOV. 2022;12(2):562–85.
19. Liu Y, Liu F, Wang C, Yan Y, Yuan X, Chu Q. Clinicopathological and molecular characteristics and treatment outcomes of SMARCA4-deficient thoracic tumors: a comprehensive analysis. Oncologist. 2025;30(9):oyaf266.
20. Zou X, Zhou X, Guo X, Pan L, Li W. SMARCA4 deficiency: implications for non-small cell lung cancer and management strategies, with relevance to and distinctions from thoracic undifferentiated tumor. TRANSL LUNG CANCER R. 2025;14(4):1456–70.
21. Liu Y, Lv T, Han L, Li Y. CT imaging features of pulmonary SMARCA4-deficient undifferentiated carcinoma: a retrospective case series. FRONT ONCOL. 2026;16:1822031.

Figures

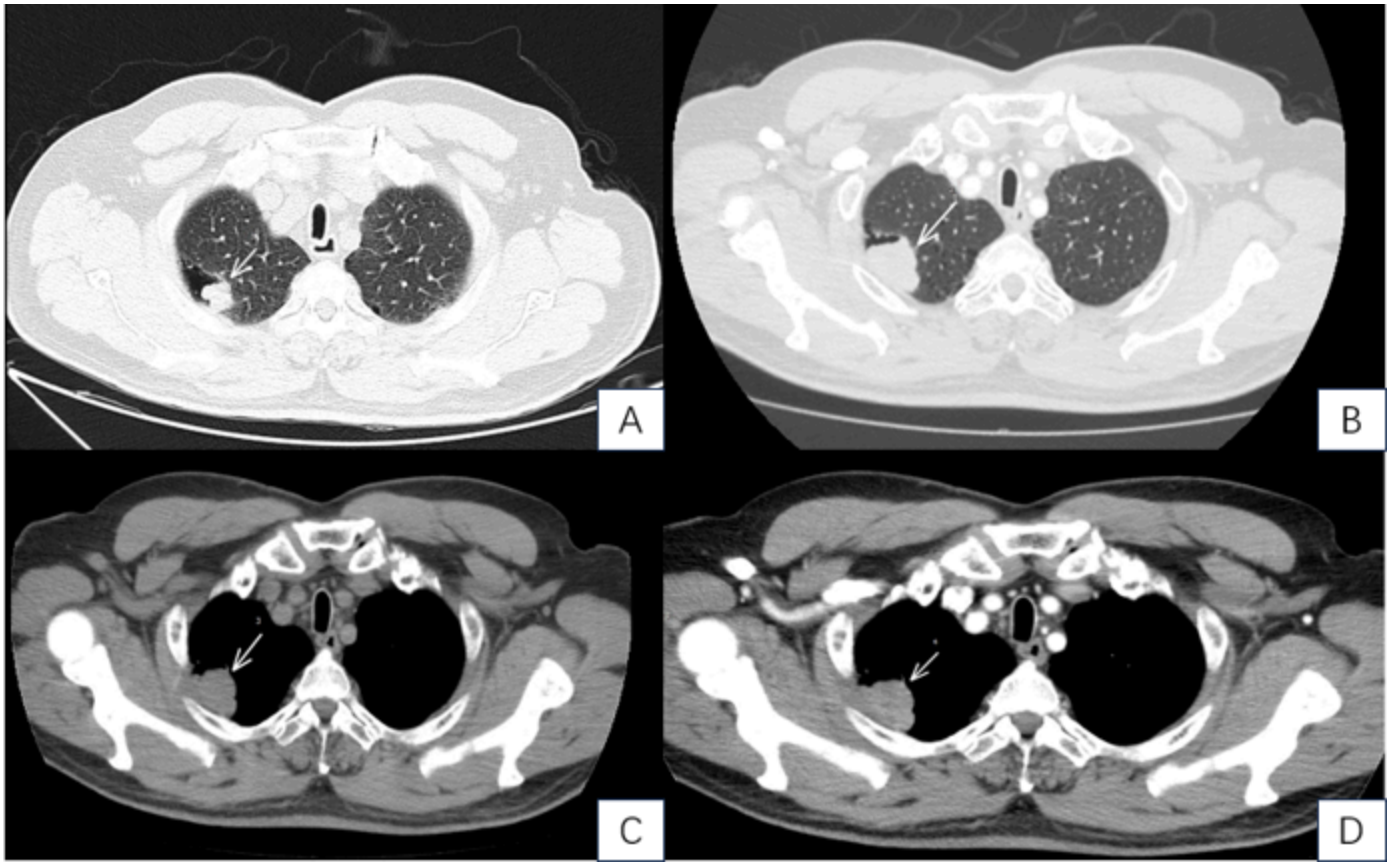


Figure 1

Images from a 62-year-old man with a 45-year history of smoking 20 cigarettes per day who presented with rapid tumour growth without treatment. **(A)** Baseline axial chest CT lung window showing a solid lobulated nodule in the upper lobe of the right lung(white arrow); **(B)**Axial chest CT after 1 year and 5 months shows that the nodules of the upper lobe of the right lung have grown substantially, with a doubling time of 76 days(white arrow); **(C)** and **(D)** Axial mediastinal window plain scan and enhanced scan images, respectively, demonstrated mild enhancement of the mass (white arrow).

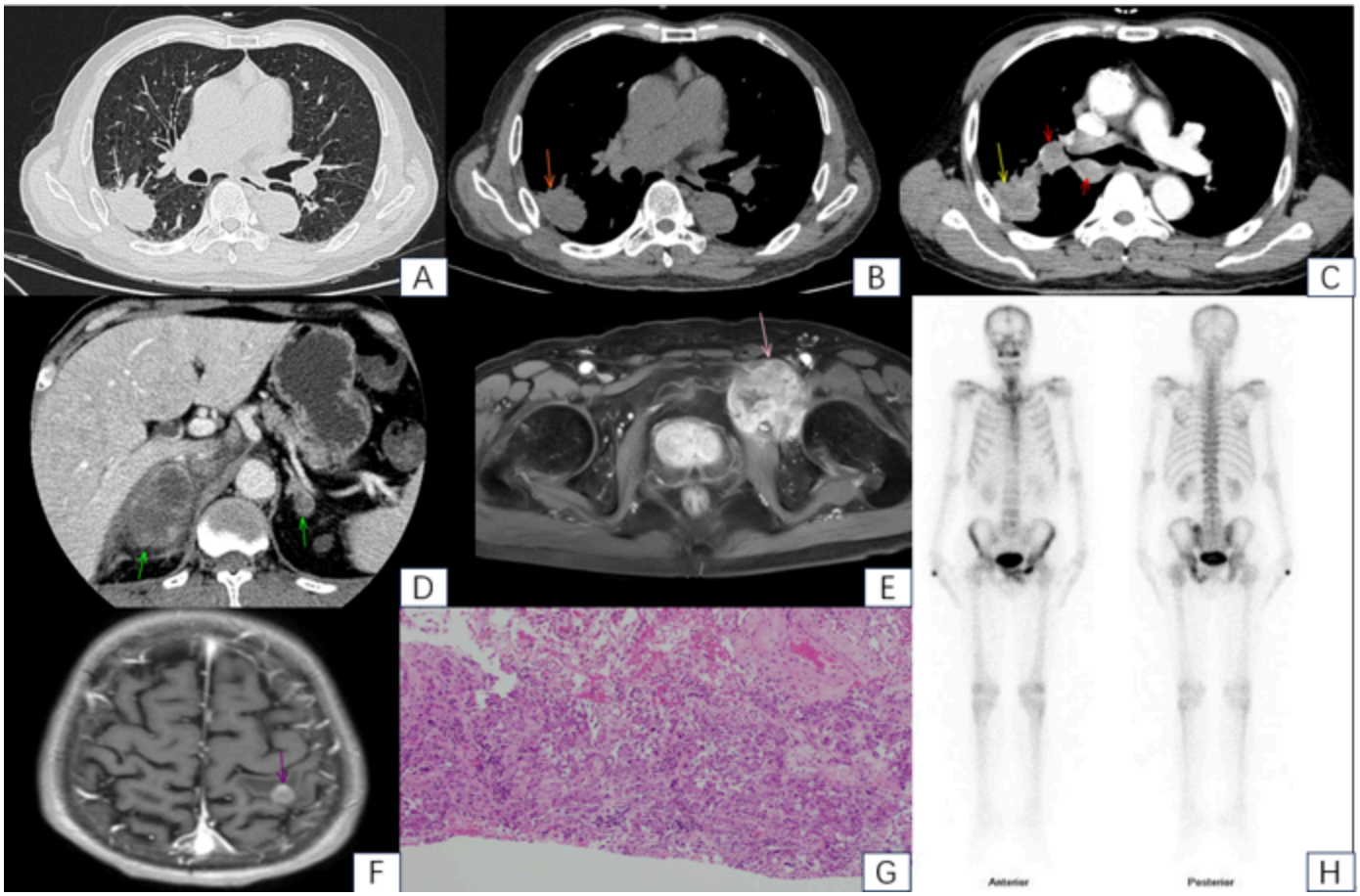


Figure 2

Images of a 69-year-old man who had smoked 40 cigarettes per day for 50 years and who presented with advanced-stage disease and local and distant metastases. (**A**) and (**B**) Axial chest CT images reveal emphysema in both lungs and a solid lobed soft tissue density mass across the upper and lower lobes of the right lung (white and red arrow). (**C**) Enhanced CT imaging shows heterogeneous enhancement with necrosis (yellow arrow). Lymph node enlargement is also visible in the right hilum of the lung (red arrow). (**D**) Bilateral adrenal nodules and masses with heterogeneous enhancement are seen on an enhanced scan image (green arrow). (**E**) Pelvic axial MRI scan reveals left pubic metastasis with significant enhancement (pink arrow). (**F**) Axial MRI scan showing metastatic tumours in the left parietal lobe (purple arrow). (**G**) Haematoxylin and eosin-stained sections. (**H**) Whole-body bone scan (WBBS) image reveals abnormal bone metabolism in the left sacroiliac joint, pubic bone, and ischiatic bone.

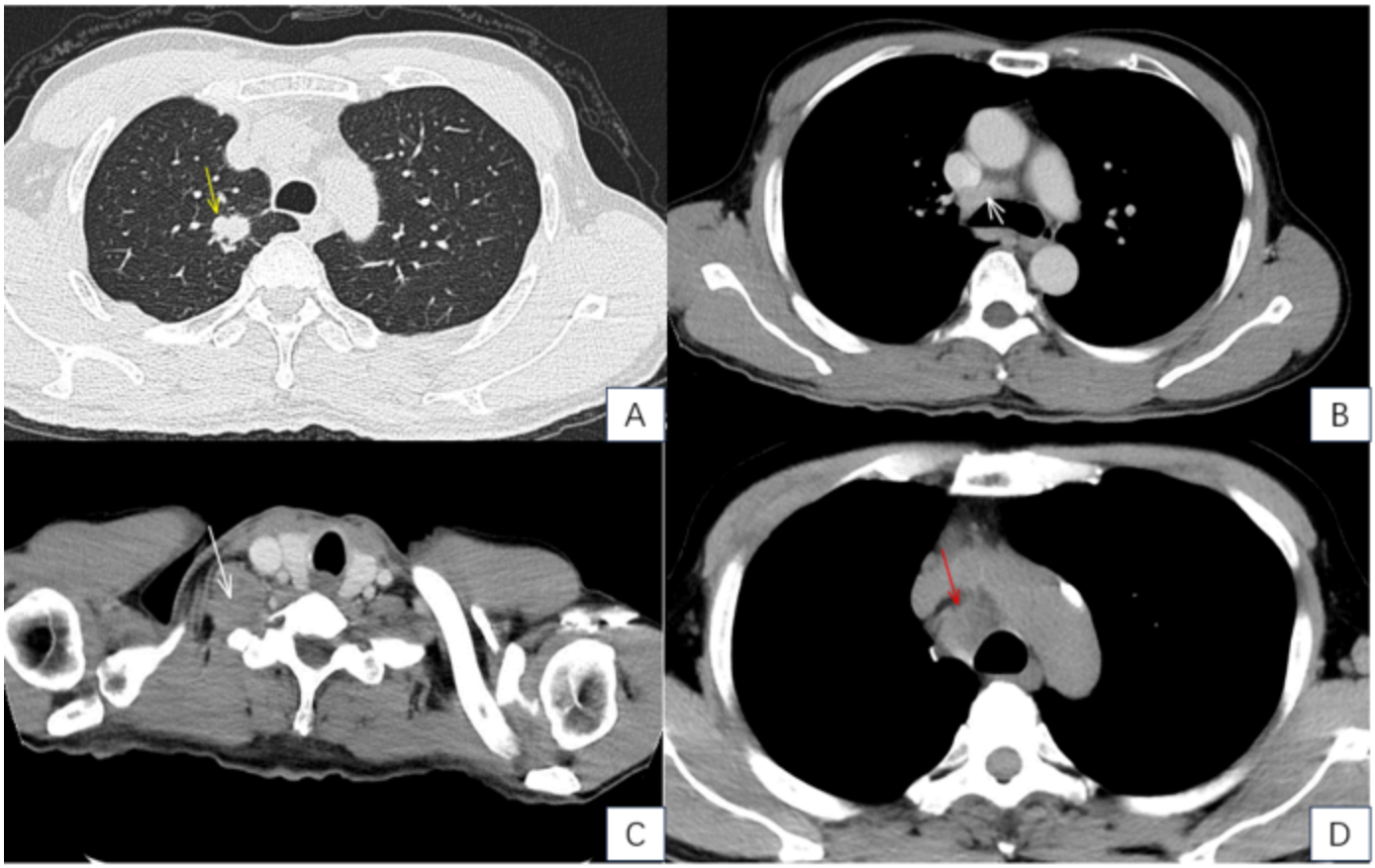


Figure 3

Images of a 62-year-old man who had smoked 30 cigarettes per day for more than 30 years and who presented with disease progression postoperatively. (**A**) Axial chest CT image showing solid lobulated nodules (yellow arrow) in the upper tip of the right lung. (**B**) Mediastinal lymph node enlargement. (**C**) Enlargement of the right supraclavicular fossa lymph nodes. (**D**) Images taken six months after right upper lobe resection and mediastinal and hilar lymph node dissection. Axial chest CT reveals mediastinal lymph node enlargement (red arrow), indicating tumour progression.

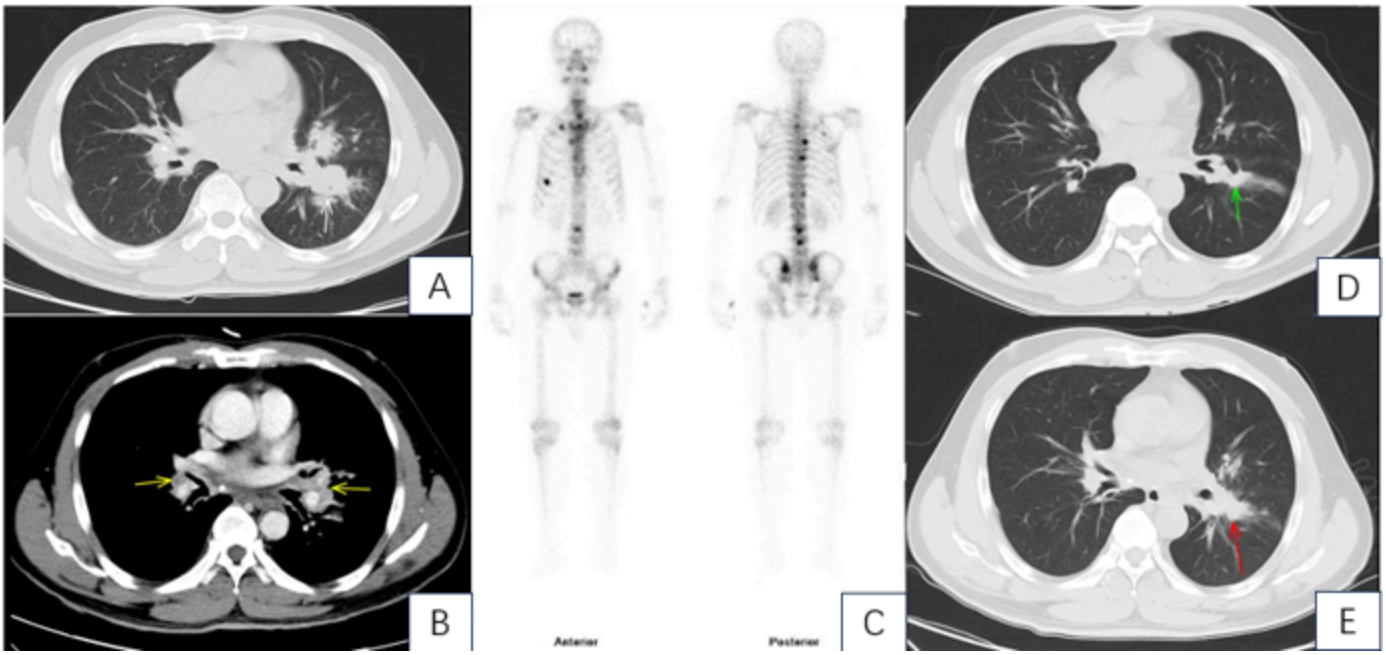


Figure 4

Images of a 52-year-old man who had smoked 30 cigarettes per day for more than 30 years and experienced partial remission (PR) after treatment and tumour progression after continued treatment. (**A**) Axial chest CT image showing a solid lobulated mass in the left lower lobe (white arrows). (**B**) Axial enhanced CT image showingmultiple enlarged lymph nodes in both pulmonary hilar regions (yellow arrow). (**C**) Whole-body bone scan (WBBS) showing multiple radioactive concentrations in the spine, bilateral ribs, and bilateral sacroiliac joints, considering bone metastases. (**D**). Chest CT examination six months after anti-bone metastasis treatment with zoledronic acid indicates significant tumour shrinkage (green arrow). (**E**) Chest CT reexamination 5 months after continued treatment indicates tumour enlargement and disease progression (red arrow).